LUNAR GEOLOGY

A sample of the Moon's far side retrieved by Chang'e-6 contains 2.83-billion-year-old basalt

Zexian Cui[1]†, Qing Yang[1]†, Yan-Qiang Zhang[1], Chengyuan Wang[1], Haiyang Xian[2], Zhiming Chen[1,3], Zhiyong Xiao[4], Yuqi Qian[5,6], James W. Head III[7], Clive R. Neal[8], Long Xiao[9], Fanglu Luo[4], Jingyou Chen[1], Pengli He[1], Yonghua Cao[2], Qin Zhou[10], Fangfang Huang[1], Linli Chen[1], Bo Wei[2], Jintuan Wang[1], Ya-Nan Yang[1], Shan Li[2,3], Yiping Yang[2], Xiaoju Lin[2], Jianxi Zhu[2], Le Zhang[1]*, Yi-Gang Xu[1]*

Remote sensing observations have shown that the far side of the Moon (lunar farside) has different geology and rock composition to those of the nearside, including the abundances of potassium, rare earth elements, and phosphorus (collectively known as KREEP). The Chang'e-6 (CE-6) spacecraft collected samples from the South Pole–Aitken (SPA) basin on the farside and brought them to Earth. We used lead-lead and rubidium-strontium isotope systems to date low-titanium basalt in a CE-6 sample, finding a consistent age of 2830 (±5) million years. We interpret this as the date of volcanism in SPA and incorporate it into lunar crater chronology. Strontium, neodymium, and lead isotopes indicate that the volcanic magma was from a lunar mantle source depleted in incompatible elements and containing almost no KREEP component.

The Moon has a global dichotomy, with its near and far sides having different geomorphology, topography, chemical composition, crustal thickness, and evidence of volcanism (*1*–*3*). Volcanic eruptions flooded parts of the surface with lava, producing rocks known as mare basalts, which are more common on the nearside (*4*), where they cover ~30% of the surface compared with 2% of the farside (*5*). Analysis of samples retrieved by the Apollo and Luna missions has indicated that most mare volcanism on both sides ceased before ~3.0 billion years (Ga) ago (*6*). Samples returned by the Chang'e-5 (CE-5) mission demonstrate that mare volcanism continued to at least 2.0 Ga ago in the Procellarum KREEP Terrane (PKT) region of the near side (*7*, *8*), and other forms of volcanism potentially continued to ~120 million years (Ma) ago (*9*, *10*). Because of a lack of samples, it is unclear when mare volcanism ceased on the farside. The SPA basin, located on the lunar farside, is the largest and oldest known lunar impact basin. Its formation is thought to have had a global effect on the Moon (*11*, *12*). Samples from the SPA basin could potentially provide information on the Moon's global dichotomy (*13*).

The CE-6 mission collected a total of 1935.3 g of lunar soil from the lunar farside and brought it to Earth for laboratory analysis. The CE-6 landing site (at lunar coordinates 41.625°S, 153.978°W) (Fig. 1) was in the southern part of the Apollo impact basin, located northeast of the SPA basin (*14*). The Apollo basin has a diameter of 492 km, making it the largest impact structure within the SPA basin, and formed earlier than 3.9 Ga ago (*15*–*17*). Remote sensing observations show that at least two episodes of mare basalt eruptions occurred in the region (Fig. 1A) (*14*, *18*–*20*). The earlier episode occurred during the Imbrian geologic period (3.3 to 3.4 Ga ago) and erupted low–titanium (Ti) basalts, likely covering the entire southern Apollo basin, which has low topography (*19*). It was followed by younger (2.4 to 3.1 Ga old) eruptions of intermediate-Ti mare basalt from the west of the previous eruption (*19*). The CE-6 samples were collected from the intermediate-Ti mare unit, close to its eastern boundary, ~5 km from the low-Ti basalt flows (Fig. 1A). We therefore expected the CE-6 samples to be dominated by the younger mare eruption.

We analyzed basalt clasts (rock fragments formed on the Moon's surface by space weathering) (Fig. 2, A and B, and fig. S1) from a CE-6 sample using radiometric dating to determine the age of the farside mare basalts. We also conducted a geochemical analysis to characterize the magma source of the eruptions.

Sample description

Thirty-five basalt clasts with sizes from 0.2 to 5 mm were identified from a 2-g aliquot of CE-6 lunar soil (scooped sample CE6C0100YJFM003) and analyzed with a scanning electron microscope (SEM) (*21*). Using electron probe microanalysis (EPMA), we identified grains of pyroxene in these basaltic clasts (*21*), which follow two compositional trends (fig. S2A). The pyroxene compositions are expressed as the molar ratios Ti# ≡ 100 × Ti/(Ti + Cr) and Fe# ≡ 100 × Fe/(Fe + Mg). Thirty-three of the 35 basaltic clasts follow a monotonic trend, beginning from a low-Ti composition (which we interpret as the parent magma) and extending to higher Ti# and Fe#. The other two clasts have much lower Ti content, so we inferred that they formed from a very low-Ti (VLT) parental magma. Pyroxene in all 35 clasts has iron/manganese (Fe/Mn) ratios similar to previous measurements of nearside mare basalts (fig. S2B). The mineral assemblages in both groups are similar; we identified minerals including plagioclase, pyroxene, ilmenite, and troilite. The low-Ti basalt contains more ilmenite (~5%) than did the VLT basalt (<1%) (Fig. 2, A and B). This provides petrographic support for our interpretation that there are two types of mare basalts in the sample. The predominance of low-Ti basalts in our clasts most likely represents the local basalts (*19*) that formed during the Eratosthenian period (3.2 to 0.8 Ga ago) (*22*, *23*).

Fractures are common in these basaltic clasts, whereas shock veins and melt pockets are absent. Some datable minerals are present, mostly in the mesostasis (the last minerals to crystallize in lunar basalts) area of the low-Ti group, including apatite (size, 10 to 50 μm), baddeleyite (size, 3 to 20 μm), and tranquillityite (size, 4 to 15 μm) (Fig. 2, C and D; fig. S1; and data S2). No phosphates or zirconium (Zr)–bearing minerals were found in the two VLT basaltic clasts. We therefore performed isotopic dating on the low-Ti basaltic clasts only.

Radioisotope dating

The 33 low-Ti basaltic clasts were used for lead (Pb) isotope measurements (data S3). Zr-bearing minerals (number of analyses, *n* = 44), apatite (*n* = 78), potassium (K)–rich phases (K-feldspar and K-glass; *n* = 54), and troilite (*n* = 11) were analyzed in a secondary ion mass spectrometer by using a primary beam of oxygen ions (O^-) with ~3-, ~5-, ~15-, and ~15-μm spot sizes, respectively (fig. S3). From the 187 individual measurements, 60 were discarded for having elevated $^{204}Pb/^{206}Pb$ ratios, which indicates terrestrial contamination (*21*). The remaining 127 measurements were used to construct a Pb-Pb isochron (line of constant age) (Fig. 3A). Fitting a linear model to the data indicated a mean age of 2830 ± 5 Ma [mean squared weighted deviation (MSWD) = 0.53, 95% confidence level].

In 17 of the low-Ti basaltic clasts, we identified clean grains of plagioclase—those that are free of mineral inclusions, mesostasis pockets, or mesostasis domains—making them suitable

---

[1]State Key Laboratory of Isotope Geochemistry, Guangzhou Institute of Geochemistry, Chinese Academy of Sciences, Guangzhou, China. [2]CAS Key Laboratory of Mineralogy and Metallogeny, Guangzhou Institute of Geochemistry, Chinese Academy of Sciences, Guangzhou, China. [3]College of Earth and Planetary Sciences, University of Chinese Academy of Sciences, Beijing, China. [4]Planetary Environmental and Astrobiological Research Laboratory, School of Atmospheric Sciences, Sun Yat-sen University, Zhuhai, China. [5]Department of Earth Sciences, The University of Hong Kong, Hong Kong, China. [6]GIGCAS-HKU Joint Laboratory of Chemical Geodynamics, The University of Hong Kong, Hong Kong, China. [7]Department of Earth, Environmental, and Planetary Sciences, Brown University, Providence, RI, USA. [8]Department of Civil and Environmental Engineering and Earth Sciences, University of Notre Dame, Notre Dame, IN, USA. [9]State Key Laboratory of Geological Processes and Mineral Resources, Planetary Science Institute, School of Earth Sciences, China University of Geosciences, Wuhan, China. [10]State Key Laboratory of Organic Geochemistry, Guangzhou Institute of Geochemistry, Chinese Academy of Sciences, Guangzhou, China.
***Corresponding author. Email: yigangxu@gig.ac.cn (Y.-G.X.); zhangle@gig.ac.cn (L.Z.)**
†These authors contributed equally to this work.

for analysis of rubidium-strontium (Rb-Sr) isotopes (fig. S4). A total of 32 clean plagioclase grains and 27 plagioclase grains with various amounts of late-stage mesostasis (data S4) were measured by using multiple-collector inductively coupled plasma mass spectrometry (MC-IPMS) (*21*). The Rb-Sr measurements of grains with mesostasis domains and clean plagioclase followed a single isochron, with the clean plagioclase close to the initial ratio (Fig. 3B). The Rb-Sr isochron had a fitted model age of 2839 ± 95 Ma (MSWD = 2.3, 95% confidence level) and initial ^{87}Sr/^{86}Sr ratio of 0.69927 ± 0.00004 (2σ). This Rb-Sr age is consistent with (but less precise than) that derived from the Pb-Pb measurements.

The consistent ages and pyroxene composition (fig. S2B) indicate that the measured low-Ti basaltic clasts probably have a common origin. We adopt the higher precision Pb-Pb age of 2830 ± 5 Ma and interpret it as the crystallization age of the low-Ti basalt unit. This is older than the 2.0-Ga-old basalt sampled by CE-5 (*7*, *8*) but demonstrates that volcanism occurred more recently than 3.0 Ga ago on both the near- and farsides of the Moon.

Origin of the parent magma

We considered the intermediate-Ti and low-Ti basalt units, identified with remote sensing, as likely corresponding to the low-Ti and VLT basalts in our sample, respectively, on the basis of their pyroxene compositional trends (fig. S2). Those trends indicate that extensive evolution of the parent magmas increased the titanium dioxide (TiO_2) contents of the erupted lava to the low-Ti and intermediate-Ti categories (*19*). The Ti abundances we measured in the pyroxene grains are lower (data S1 and fig. S2A) than we expected from the remote sensing data (Fig. 1C).

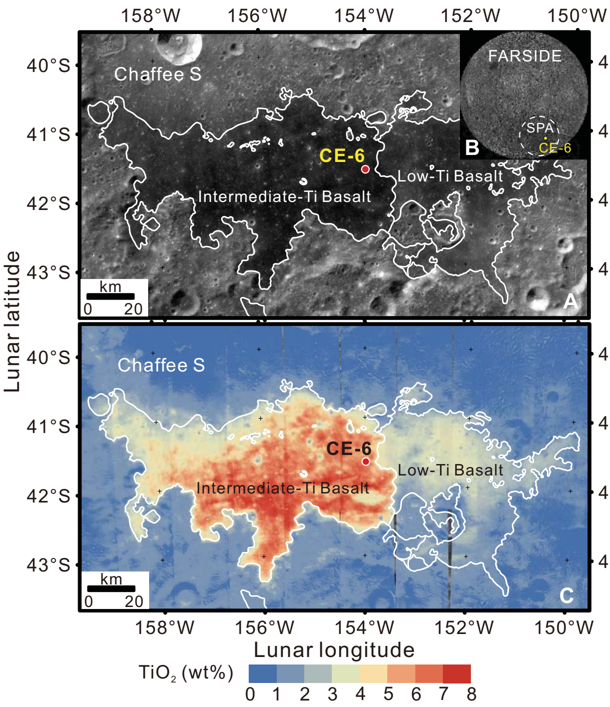

Fig. 1. Geological settings of the CE-6 landing site. (**A**) Location of the CE-6 landing site (red dot) in the south of Apollo basin. The background image is an orthographic albedo map from Chang'e-2 (*36*). (**B**) Zoom out of the entire farside hemisphere. The yellow dot indicates the CE-6 landing site, and the white dashed circle outlines the SPA basin. (**C**) TiO_2 abundance map [color bar in weight percent (wt %)] of the same region as in (A), derived from Kaguya Multiband Image data (*37*). In (A) and (C), the younger basalts are labeled intermediate-Ti, and the older basalts are labeled low-Ti. The white lines indicate the boundary of mare units.

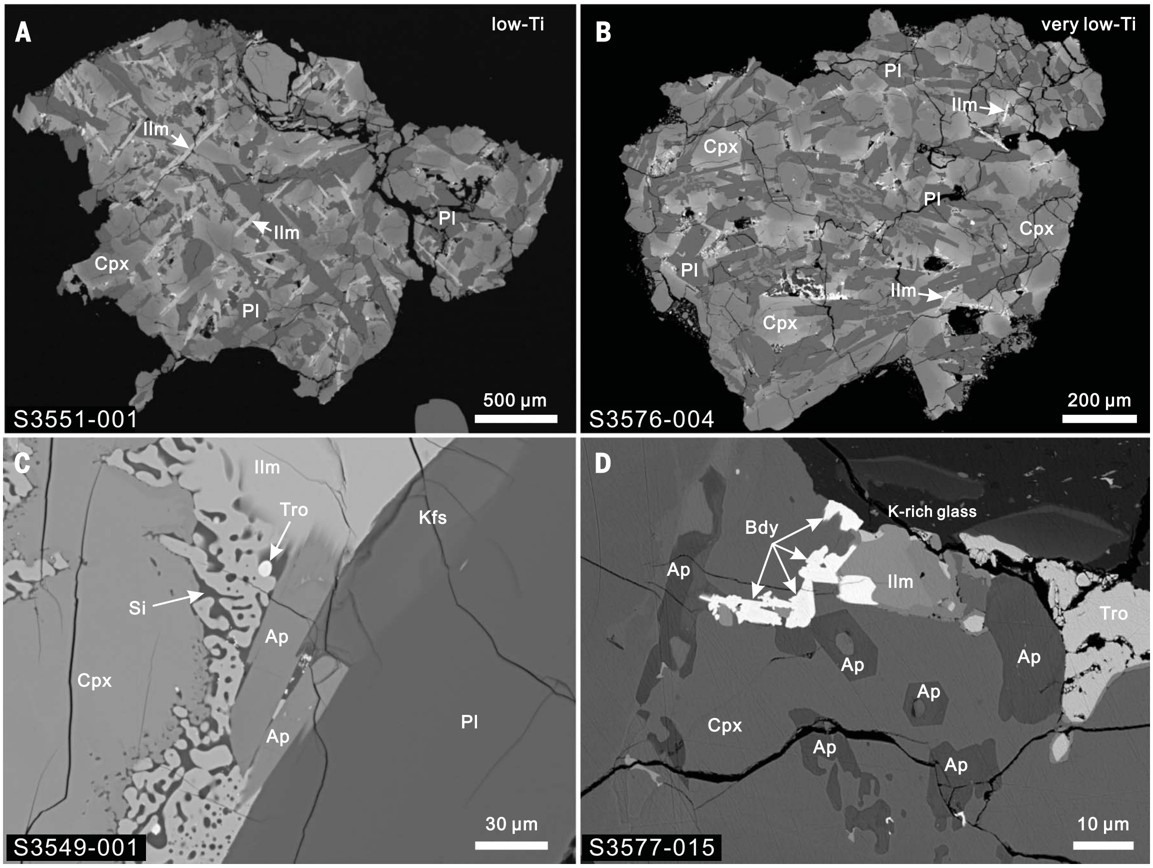

Fig. 2. Two types of basaltic clasts in CE-6 lunar soil. Backscattered electron (BSE) images of two clasts, with mineral phases labeled. The brightness and contrast vary between images. (**A**) Low-Ti basalt clast with moderate content of ilmenite. (**B**) Very low-Ti basalt clast with much less ilmenite. (**C** and **D**) Zoomed regions of two other low-Ti basalt clasts. Fine apatite, baddeleyite, and potassium-rich phases are labeled. (A) to (D) are labeled with the resin mount number [S3551 in (A)] and the particle number [001 in (A)]. Mineral abbreviations are Pl, plagioclase; Cpx, clinopyroxene; Ilm, ilmenite; Ap, apatite; Tro, troilite; Bdy, baddeleyite; Kfs, K-feldspar; and Si, silica.

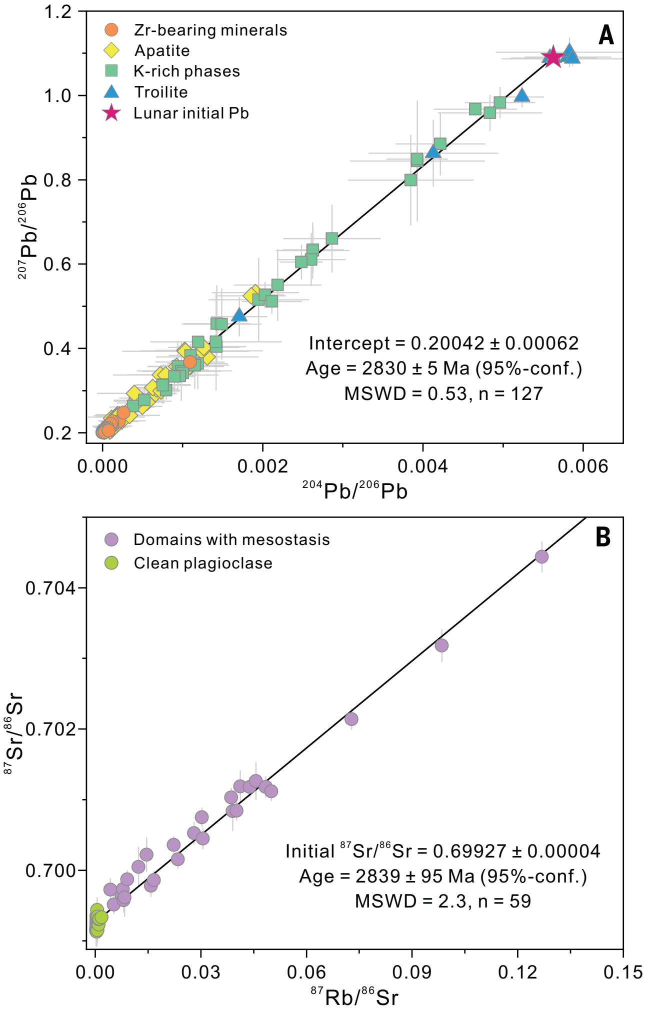

Fig. 3. Radioisotope dating of the CE-6 low-Ti basaltic clasts. Plotting symbols indicate measurements from different mineral phases. Error bars are 2σ. (**A**) Pb-Pb istopes in 33 low-Ti basaltic clasts. Measurements discarded because of terrestrial Pb contamination are omitted here but are shown in fig. S3A. (**B**) Rb-Sr isotopes for 17 low-Ti basaltic clasts.

We regard this discrepancy as being likely due to the very different sampling scales. The remote sensing TiO_2 measurement is an average value of a large area (20 m $pixel^{-1}$) (Fig. 1B), whereas the scooped soil sample collected by CE-6 was from an area of less than 1 m^2. Although we conclude that the low-Ti basaltic clasts are representative of the mare basalts local to the sampling site (*21*), we are unable to determine the provenance of the VLT clasts. They could be derived from the older mare unit to the east of the CE-6 landing site (Fig. 1A), or be fragments of underlying mare units that were excavated to the surface by impacts, or were transported to the sample site from more distant locations (*19*).

It has been suggested that lunar magmatism was sustained by radiogenic heating from KREEP components in the mantle sources of the magmas (*24*). However, studies of CE-5 basalt (*25*) and some ~3.0-Ga-old lunar meteorites (*26*) have found that these younger basalts do not contain a KREEP component. Because the CE-6 low-Ti basalt records similarly young basaltic volcanic activity on the farside, we investigated whether the mantle source contained a KREEP component by examining the initial strontium-neodymium (Sr-Nd) isotopic compositions and initial $^{238}U/^{204}Pb$ ratio (μ value).

We selected the five analyses of troilites in the CE-6 basaltic clasts that have the highest measured $^{207}Pb/^{206}Pb$ ratios (data S2), 1.090 ± 0.007 (2σ), which we assume represents the initial $^{207}Pb/^{206}Pb$ composition. The initial $^{204}Pb/^{206}Pb$ ratio is more difficult to determine because of the low current abundance of ^{204}Pb. We therefore constrained the initial $^{204}Pb/^{206}Pb$ ratio using the estimated initial $^{207}Pb/^{206}Pb$ and the best-fitting Pb-Pb isochron (Fig. 3A), which yields an initial $^{204}Pb/^{206}Pb$ of 0.00563 ± 0.00013 (2σ). We then used a two-stage lunar Pb isotopic evolution model (*27*) to estimate the μ value of the CE-6 low-Ti basalt mantle source. The model assumes that the Moon formed at 4500 Ma ago and evolved as a single body, with initial Pb isotopes equal to the isotopic standard Canyon Diablo Troilite (*28*) and had a μ value of 460. Beginning at 4376 Ma ago in the model, the Moon differentiated to produce different mantle sources (*27*). Our application of this model indicates a μ value of 355 ± 8 for the CE-6 low-Ti basalt mantle source (Fig. 4A). This is much lower than the μ values of KREEP-rich basalts [>2000 (*27*)] and the PKT basalt from CE-5 [~680 (*7*, *8*)].

The 32 clean plagioclase measurements yielded an average initial $^{87}Sr/^{86}Sr$ ratio of 0.69922 ± 0.00013 (2σ), which is consistent with the initial ratio determined from the fitted Rb-Sr isochron (0.69927 ± 0.00004, 2σ) and lower than those of CE-5 basalts and most Apollo mare basalts (fig. S5A). We measured samarium-neodymium (Sm-Nd) isotopic compositions of domains containing late-stage mesostasis with high proportions of apatite in the CE-6 low-Ti basalt (fig. S4 and data S5). We found that the $^{147}Sm/^{144}Nd$ ratios vary from 0.2049 to 0.2384 and $^{143}Nd/^{144}Nd$ ratios vary from 0.51370 ± 0.00007 (2σ) to 0.51424 ± 0.00013 (2σ). The averaged initial ε_{Nd} (defined in eq. S1) is 17.2 ± 2.4 (2σ, n = 8), which is higher than that of other lunar samples (fig. S5B).

We calculated the expected evolution of the depleted mantle and urKREEP (primordial KREEP from the lunar magma ocean) using an initial $^{87}Sr/^{86}Sr$ of 0.69903 and a chondrite-like initial $^{143}Nd/^{144}Nd$. For the depleted mantle, $^{87}Rb/^{86}Sr$ and $^{147}Sm/^{144}Nd$ were set to 0.005 and 0.286, respectively. For urKREEP, they were set to 0.206 and 0.158, respectively, fitted to the plotted lunar samples in Fig. 4B, which shows that the initial Sr-Nd isotopes of the CE-6 low-Ti basalt are compatible with our calculated Sr-Nd isotopic evolution trajectory for depleted lunar mantle with $^{87}Rb/^{86}Sr$ = 0.005 and $^{147}Sm/^{144}Nd$ = 0.286. The initial Sr-Nd-Pb isotopes of the CE-6 low-Ti basalt indicate a mantle source depleted in incompatible elements (elements that tend to remain in melts during partial melting or crystallization), containing no measurable KREEP component. The farside CE-6 low-Ti basalts, and nearside CE-5 basalts, indicate that heat-producing KREEP components were probably not responsible for the generation of their parent magmas.

It has been suggested that the asymmetry of lunar nearside and farside volcanic activity is due to differences in the thickness of the Moon's crust (*4*, *29*). The farside has a thicker crust (mean ~50 km compared with ~30 km on the nearside) (*30*), which could explain the lower level of volcanism. However, the SPA basin on the farside has a crust that is thinner (20 to 30 km) (*30*) than the mean but that still does not contain abundant mare basalts. The giant impact basins on the nearside, such as Imbrium, Serenitatis and Tranquillitatis, are all flooded by mare basalts, whereas the SPA basin, the largest lunar impact basin, contains few volcanic deposits (*18*).

The Sr-Nd-Pb isotopic signature of the CE-6 low-Ti basalt indicates that it was sourced from a non-KREEP mantle source, whereas KREEP is widespread on the nearside. The very depleted mantle source could be related to the impact that formed the SPA basin, which had

Fig. 4. Initial Sr-Nd-Pb isotopes of lunar basalts. (**A**) Initial $^{206}Pb/^{204}Pb$ as a function of crystallization age for lunar basalts from Apollo and Chang'e samples and lunar meteorites. The dashed lines indicate calculated evolution trajectories from a two-stage Pb isotope evolution model (*27*) of different lunar mantle sources at varying μ values. Our CE-6 measurement (red star) is compared with CE-5, Apollo, and meteorite data (*8*, *27*, *38*). (**B**) Initial ε_{Nd} as a function of initial $^{87}Sr/^{86}Sr$ for lunar basalts and meteorites. The dashed lines indicate evolutionary models calculated as described in the main text. Data sources are CE-5 basalt, (*25*); Apollo basalts, (*39*, *40*); and lunar meteorites, (*26*, *38*, *41*–*44*).

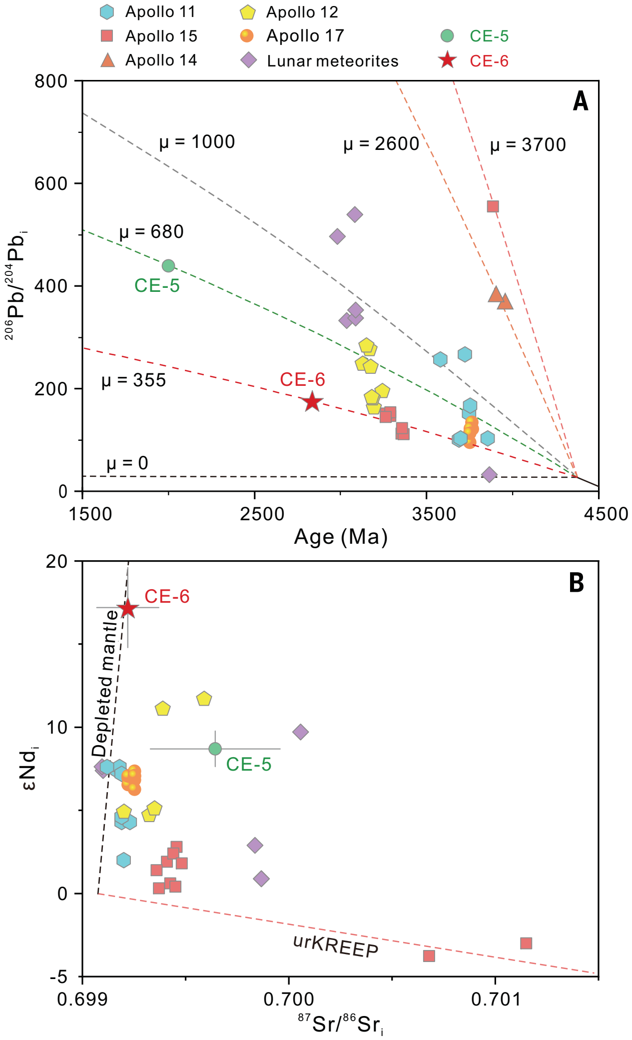

an excavation depth of 100 km (*31*). The SPA impact might have redistributed any subcrustal KREEP material to the nearside of the Moon (*11*, *12*) and induced partial melting of the mantle beneath the SPA basin, leaving a depleted mantle below SPA with low uranium (U)/Pb and Rb/Sr ratios and a high Sm/Nd ratio (fig. S6). Over time, Sr, Nd, and Pb isotopic ratios evolved owing to radioactive decay until they matched the isotopic compositions that we measured for the CE-6 low-Ti basalts. Depleted mantle material would have a higher melting-point temperature than that of mantle material that did contain a KREEP component (*32*). KREEP contains elements that generate heat through radioactivity [including K, thorium (Th), and U], so the absence of KREEP in the CE-6 mantle source would correspond to a low heat flow in the SPA basin. We suggest that a combination of these factors could explain the rarity of mare volcanism in the SPA basin.

Implications for lunar crater chronology

Isotopic dating provides absolute ages for locations on the Moon from which samples have been retrieved. The ages of other locations are indirectly estimated from the number and size of impact craters, calibrated to the locations with measured absolute ages. Models of this lunar crater chronology have shown that the impact rate on the Moon has varied over time (*33*). The lunar impact flux was high at early times and then rapidly declined to a nearly constant rate, but timing of that transition is poorly constrained. The canonical chronology model predicts that the transition occurred ~3.0 Ga ago (*33*). However, the only absolute age available between ~3.0 to 0.8 Ga ago was the CE-5 basalts (*7*, *8*). Our isotopic dating of the CE-6 mare basalt provides an additional calibration point at ~2.8 Ga ago.

Adding the CE-6 data point to a crater chronology model requires a determination of $N(1)$, the spatial density of impact craters with diameter $D \geq 1$ km, at the landing site. Before the launch of CE-6, predictions for the age of the landing site ranged from 2.42 to 3.33 Ga (*5*, *14*, *19*, *34*) because of differences in the determinations of $N(1)$. We adopted $N(1) = (2.01 \pm 0.90) \times 10^{-3}$ km^{-2} from a study (*35*) of craters with diameters ~200 m to 2 km in multiple areas of the mare beneath the CE-6 landing site. We discuss this choice of $N(1)$ in the supplementary text.

Using the measured date and $N(1)$ value for the CE-6 landing site, we recalibrated the lunar crater chronology model using least square fitting (Fig. 5A). We found

$$N(1) = (1.94 \times 10^{-14})(e^{7.196t} - 1) + (7.652 \times 10^{-4})t \quad (1)$$

where t is time in billion years. This chronology model implies a constant impact flux after 2.83 Ga ago, which is slightly earlier than the canonical model (Fig. 5B).

REFERENCES AND NOTES

1. A. M. Gaffney *et al.*, *Rev. Mineral. Geochem.* **89**, 103–145 (2023).
2. B. L. Jolliff, J. J. Gillis, L. A. Haskin, R. L. Korotev, M. A. Wieczorek, *J. Geophys. Res.* **105** (E2), 4197–4216 (2000).
3. C. Shearer *et al.*, *Rev. Mineral. Geochem.* **89**, 147–206 (2023).
4. J. W. Head III, L. Wilson, *Geochim. Cosmochim. Acta* **56**, 2155–2175 (1992).
5. J. Zhao *et al.*, *Space Sci. Technol.* **3**, 0076 (2023).
6. T. Morota *et al.*, *Earth Planet. Sci. Lett.* **302**, 255–266 (2011).
7. X. Che *et al.*, *Science* **374**, 887–890 (2021).
8. Q.-L. Li *et al.*, *Nature* **600**, 54–58 (2021).
9. B.-W. Wang *et al.*, *Science* **385**, 1077–1080 (2024).
10. S. E. Braden *et al.*, *Nat. Geosci.* **7**, 787–791 (2014).
11. M. J. Jones *et al.*, *Sci. Adv.* **8**, eabm8475 (2022).
12. N. Zhang *et al.*, *Nat. Geosci.* **15**, 37–41 (2022).
13. B. Jolliff *et al.*, *Bull. Am. Astron. Soc.* **53**, 290 (2021).
14. X. Zeng *et al.*, *Nat. Astron.* **7**, 1188–1197 (2023).
15. H. Hiesinger *et al.*, *J. Geophys. Res. Planets* **117**, E00H10 (2012).
16. M. A. Ivanov *et al.*, *J. Geophys. Res. Planets* **123**, 2585–2612 (2018).
17. C. Orgel *et al.*, *J. Geophys. Res. Planets* **123**, 748–762 (2018).
18. J. H. Pasckert, H. Hiesinger, C. H. van der Bogert, *Icarus* **299**, 538–562 (2018).
19. Y. Qian *et al.*, *Earth Planet. Sci. Lett.* **637**, 118737 (2024).
20. X. Wang *et al.*, *J. Geophys. Res. Planets* **129**, e2023JE008176 (2024).
21. Materials and methods are available as supplementary materials.
22. D. Stöffler, G. Ryder, in *Chronology and Evolution of Mars*, vol. 12, R. Kallenbach, J. Geiss, W. K. Hartmann, Eds. (Springer Netherlands, 2001), pp. 9–54.
23. D. E. Wilhelms, J. F. McCauley, N. J. Trask, "The geologic history of the Moon" (Tech. Rep. 1348, US Geological Survey, 1987). DOI: 10.3133/pp1348.
24. M. Laneuville, J. Taylor, M. A. Wieczorek, *J. Geophys. Res. Planets* **123**, 3144–3166 (2018).
25. H.-C. Tian *et al.*, *Nature* **600**, 59–63 (2021).
26. S. M. Elardo *et al.*, *Meteorit. Planet. Sci.* **49**, 261–291 (2014).
27. J. F. Snape *et al.*, *Geochim. Cosmochim. Acta* **266**, 29–53 (2019).
28. C. Göpel, G. Manhès, C. J. Allègre, *Geochim. Cosmochim. Acta* **49**, 1681–1695 (1985).
29. L. Wilson, J. W. Head, *Icarus* **283**, 146–175 (2017).
30. M. A. Wieczorek *et al.*, *Science* **339**, 671–675 (2013).
31. H. J. Melosh *et al.*, *Geology* **45**, 1063–1066 (2017).
32. M. M. Hirschmann, *Geochem. Geophys. Geosyst.* **1**, 2000GC000070 (2000).
33. G. Neukum, B. A. Ivanov, W. K. Hartmann, in *Chronology and Evolution of Mars*, R. Kallenbach, J. Geiss, W. K. Hartmann, Eds. (Springer Netherlands, 2001), pp. 55–86.
34. Z. Yue *et al.*, *Innovation (Camb.)* **5**, 100663 (2024).
35. F. Luo *et al.*, *Astrophys. J. Lett.* **974**, L37 (2024).
36. X. Ren *et al.*, *European Planetary Science Congress* **9**, EPSC2014-2344 (2014).
37. M. Ohtake *et al.*, *Adv. Space Res.* **42**, 301–304 (2008).
38. R. E. Merle, A. A. Nemchin, M. J. Whitehouse, G. G. Kenny, J. F. Snape, *J. Petrol.* **65**, egae062 (2024).
39. J. B. Paces *et al.*, *Geochim. Cosmochim. Acta* **55**, 2025–2043 (1991).
40. G. A. Snyder, C. R. Neal, L. A. Taylor, A. N. Halliday, *Geochim. Cosmochim. Acta* **61**, 2731–2747 (1997).

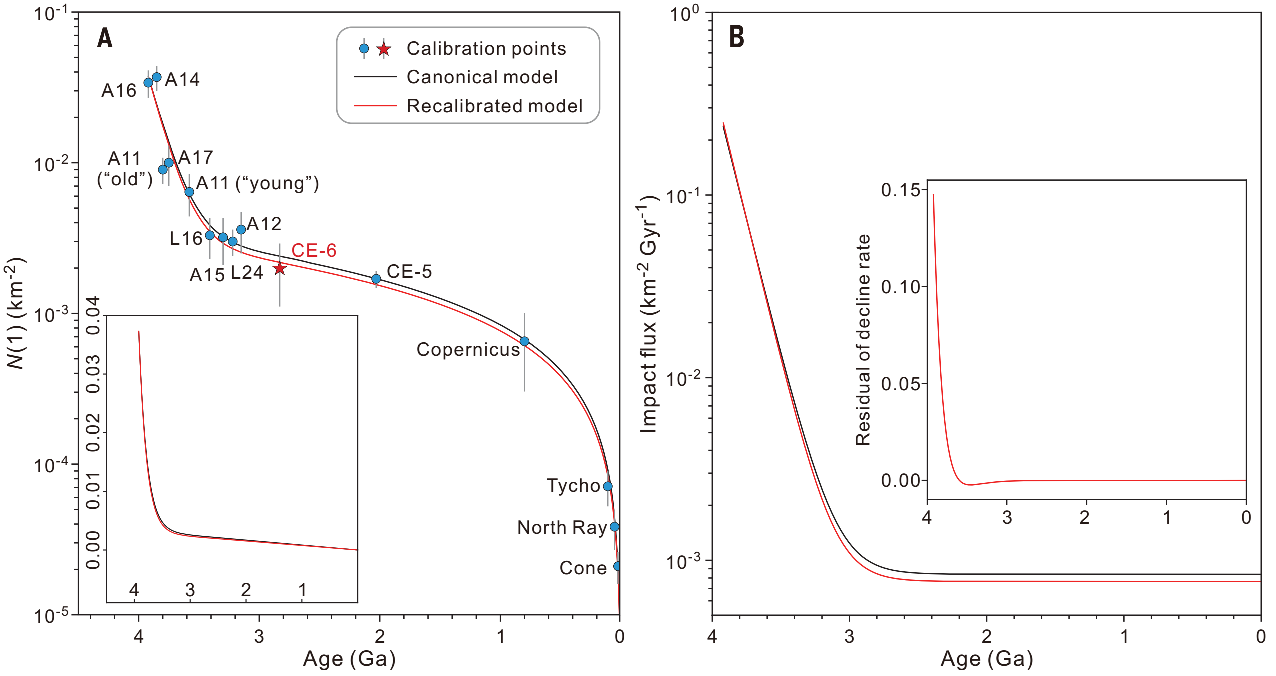

Fig. 5. Incorporating the Chang'e-6 landing site into a lunar crater chronology model. (**A**) *N*(1), the density of craters larger than 1 km, as a function of age. Blue circles are calibration points from Apollo (A11, A12, A14, A15, A16, and A17) and Luna (L24) samples by using crater densities (*15*, *45*) and radiometric ages (*22*), and from CE-5 by using the radiometric age (*8*) and crater density (*46*). The red star indicates the constraint from CE-6 by using the radiometric age (this work) and adopted crater density (*47*). Error bars indicate 1σ uncertainties. The black curve is the canonical crater chronology (*33*), and the red curve is our recalibrated model (Eq. 1). (Inset) The same models on a linear scale. (**B**) The impact flux, determined by integrating the chronology models in (A). The recalibrated model has a slightly faster decline of impact flux between 4.0 and 3.0 Ga ago and a slightly lower constant flux thereafter. (Inset) The residual between the two models.

41. L. E. Borg *et al.*, *Geochim. Cosmochim. Acta* **73**, 3963–3980 (2009).
42. L. E. Borg, C. K. Shearer, Y. Asmerom, J. J. Papike, *Nature* **432**, 209–211 (2004).
43. K. Misawa, M. Tatsumoto, G. B. Dalrymple, K. Yanai, *Geochim. Cosmochim. Acta* **57**, 4687–4702 (1993).
44. K. Rankenburg, A. D. Brandon, M. D. Norman, *Geochim. Cosmochim. Acta* **71**, 2120–2135 (2007).
45. G. Neukum, *Meteoritics* **18**, 362 (1983).
46. L. Qiao *et al.*, *Icarus* **364**, 114480 (2021).
47. China National Space Administration, Notice of China National Space Administration on the distribution of procedures for requesting lunar samples (in Chinese and English), 17 December 2020; www.cnsa.gov.cn/n6758823/n6758839/c6811124/content.html.
48. Z. Xiao, Lunar dichotomy: Chang'e-6 2.83 Ga farside mare basalts reveal most depleted mantle to date. Zenodo (2024); https://doi.org/10.5281/zenodo.13989416.

ACKNOWLEDGMENTS

We thank Y.-G. Zhang and F. Zhang for advice and comments on a draft manuscript. We thank the China National Space Administration (CNSA) for providing the CE-6 samples. We appreciate K. Joy, A. Lagain, and an anonymous reviewer for their thoughtful reviews, which helped to improve the manuscript. The lunar working group at the Guangzhou Institute of Geochemistry, Chinese Academy of Science (GIGCAS), is thanked for inspiring discussions. This is contribution no. IS-3578 from GIGCAS. **Funding:** Y.-G.X. was financially supported by the Chinese Academy of Sciences (grants XDB 1180000 and ZDBS-SSW-JSC007-11). L.Z. was supported by the lunar research program of GIGCAS (grant 2022SZJJZD-03). **Author contributions:** Y.-G.X. and L.Z. designed the project. Y.-Q.Z. and J.C. prepared the sample mounts. Z.Cu. and Q.Y. collected secondary ion mass spectrometry (SIMS) data; L.Z., Z.Ch., H.X., C.W., J.C., P.H., Y.C., Q.Z., F.H., L.C., B.W., J.W., Y.-N.Y., S.L., Y.Y., X.L. and J.Z. collected SEM data; L.Z., C.W., and J.C. collected laser ablation MC-IPMS (LA-MC-ICPMS) data. Z.Cu., L.Z., Z.Ch., J.C., Y.Q., Z.X., J.W., and F.L. produced data tables, produced figures, and performed calculations. L.Z., Y.-G.X., Z.Cu., Q.Y., J.C., Z.X., Y.Q., L.X., J.W.H., and C.R.N. drafted the manuscript. All authors revised the manuscript. **Competing interests:** We declare no competing interests. **Data and materials availability:** The lunar soil investigated in this study (CE6C0100YJFM003) was provided by the CNSA under a materials transfer agreement (*47*). The prepared sample mounts are currently held at GIGCAS on a 1-year loan, after which they will be returned to CNSA. Readers may request Chang'e-6 samples from CNSA through a standard procedure (*47*). The crater chronology data and our fitting code are available at Zenodo (*48*). Our measured compositions of pyroxene and Pb-Pb dating minerals are provided in data S1 and S2, and our measured Pb-Sr-Nd isotopes are in data S3 to S5.

SUPPLEMENTARY MATERIALS

science.org/doi/10.1126/science.adt1093
Materials and Methods
Supplementary Text
Figs. S1 to S6
References (*49*–*93*)
Data S1 to S5

Submitted 12 September 2024; accepted 8 November 2024
Published online 15 November 2024
10.1126/science.adt1093